PAPER

Check for updates

Mechanical exfoliation and electrical characterization of a one-dimensional Nb₂Se₉ atomic crystal†

Bum Jun Kim,‡[a] Byung Joo Jeong,‡[b] Seungbae Oh,[b] Sudong Chae,[b] Kyung Hwan Choi,[a] Tuqeer Nasir,[a] Sang Hoon Lee,[b] Kwan-Woo Kim,[b] Hyung Kyu Lim,[b] Ik Jun Choi,[b] Linlin Chi,[b] Sang-Hwa Hyun,[c] Hak Ki Yu, [iD][c] Jae-Hyun Lee*[c] and Jae-Young Choi [iD] *[ab]

A novel semiconductor 1D nanomaterial, Nb₂Se₉, was synthesized on a bulk scale *via* simple vapor transport reaction between niobium and selenium. Needle-like single crystal Nb₂Se₉ contains numerous single Nb₂Se₉ chains linked by van der Waals interactions, and we confirmed that a bundle of chains can be easily separated by mechanical cleavage. The exfoliated Nb₂Se₉ flakes exhibit a quasi-two-dimensional layered structure, and the number of layers can be controlled using the repeated-peeling method. The work function varied depending on the thickness of the Nb₂Se₉ flakes as determined by scanning Kelvin probe microscopy. Moreover, we first implemented a field effect transistor (FET) based on nanoscale Nb₂Se₉ flakes and verified that it has p-type semiconductor characteristics. This novel 1D material can form a new family of 2D materials and is expected to play important roles in future nano-electronic devices.

Introduction

To overcome the physical limitations of high-density integration in electronic manufacturing, it is necessary to develop novel three-dimensional (3D) device structures and study low-dimensional semiconductor nanomaterials.[1–4] It is expected that these materials will exhibit novel quantum physical characteristics and excellent electrical, optical, and mechanical properties.[2,5] Since graphene, a one-atom-thick honeycomb structure, was first separated from graphite, graphene-based applications in electronics, chemistry, and mechanics have been intensively studied due to its superior physical properties (*e.g.*, high charge carrier mobility and mechanical strength).[2,5,6] However, the development of technologies for the electronics industry, which is one of the most anticipated applications for various types of graphene-based materials, faces significant obstacles. Graphene does not have a bandgap, making it difficult to develop with transistors, as they are a basic component of electronic devices.[7,8] If the graphene is finely patterned with narrow widths, a bandgap can be formed.[7] Unfortunately, as the width of the graphene decreases, the bandgap increases and the electron mobility decreases sharply. Theoretically, if the graphene exhibits a bandgap of 0.5 eV (half the value of Si), the mobility should be smaller than that of Si.[8] Bandgap openings have also been observed in bilayer graphene with certain angles.[9] However, developing synthesis methods for large-area twisted bilayer graphene remains a significant challenge.

New 2D materials with appropriate bandgaps, including transition metal dichalcogenides (TMDCs) and black phosphorus, have recently been introduced.[3,10–12] However, their charge carrier mobilities are one-tenth to one-hundredth that of Si materials and their chemical stabilities are lower than those of conventional semiconductor materials.[3,10,11] Most importantly, similar to graphene, a dramatic reduction in the charge carrier mobility due to edge scattering may inevitable after device manufacture.[13]

Therefore, an ideal structure for overcoming these problems should be developed to replace quasi-two-dimensional conducting channels currently used in devices and minimize the reduction of electron mobility caused by defects and dangling bonds.[14–16] Carbon nanotubes (CNTs) contain sp² hybridized carbons and high electron mobility, with a range of electronic structures that can arise from the chirality of CNTs.[16] This variation can complicate the fabrication of electronic devices and result in uneven performance.

[a]SKKU Advanced Institute of Nanotechnology (SAINT), Sungkyunkwan University, Suwon, 16419, Korea. E-mail: jy.choi@skku.edu; Tel: +82-31-290-7353

[b]School of Advanced Materials Science & Engineering, Sungkyunkwan University, Suwon 16419, Korea

[c]Dept. of Materials Science and Engineering, Dept. of Energy Systems Research, Ajou University, Suwon, 16499, Korea. E-mail: jaehyunlee@ajou.ac.kr; Tel: +82-31-219-2465

† Electronic supplementary information (ESI) available. See DOI: 10.1039/c8ra07437b

‡ Equal contribution as first author to this work.

Recently, a novel family of 1D nanomaterials has been reported that adopt 3D forms of multiple single-molecular chains coupled by weak van der Waals (vdW) interactions.[17–27] For example, $Mo_6S_{9-x}I_x$, Sb_2S_3, and VS_4 exist as a single molecular chain of transition metals and sulfur and can be used in biocompatible electronic devices, optoelectronic devices, and electrochemical energy storage devices.[23,25–27] However, most related studies have been on thin films and no research on nanostructures for use as electronic channels has been reported.

In this study, we synthesized a 1D semiconductor nanomaterial, Nb_2Se_9, on a bulk scale *via* simple vapor transport.[28–30] The as-grown needle-like single crystal Nb_2Se_9 contains numerous single Nb_2Se_9 chains linked by vdW interactions. It was confirmed that the bundle of chains can be easily separated by mechanical cleavage. Interestingly, the isolated Nb_2Se_9 flakes exhibit a quasi-two-dimensional layered structure. The variation of the work function depends on the thickness of the Nb_2Se_9 flakes, as determined by scanning Kelvin probe microscopy (SKPM) measurements. Moreover, we first implemented a field effect transistor (FET) based on nanoscale Nb_2Se_9 flake and verified that it has p-type semiconductor characteristics.

Results and discussion

The valence electrons of the transition metal niobium exist in the 4d orbital, allowing the formation of various compounds (*e.g.*, from Nb_2Se to Nb_2Se_9) upon reaction with selenium (Fig. S1 in ESI†). Therefore, to accurately determine the stoichiometry of high-purity and high crystallinity Nb_2Se_9, the ratio of Nb : Se and reaction temperature were considered. For the atomic mixing ratio of Nb to Se powder of exactly 2 : 9, unwanted phases such as $NbSe_3$ and $NbSe_2$ can form due to the unpredictable fluctuation of Nb and Se at the reaction tube.

Based on the lever-rule, the mixing ratio was adjusted until the single crystal Nb_2Se_9 was synthesized with an exact stoichiometry ratio of 2 : 9 by adding an excess of Se, as shown in Fig. 1(a) (atomic mixing ratio of Nb to Se of 2 : 18). The crystal structure of the bulk Nb_2Se_9 crystal was investigated by X-ray diffraction (XRD) and the Nb_2Se_9 phase formed under the optimal growth conditions (JCPDS card 33-0968). The SEM images in Fig. 1(c) and (d) clearly show the needle-like wire structures and the torn 1D Nb_2Se_9 bundles generated during sample preparation.

To examine the characteristics of the layered structure of the Nb_2Se_9, the bulk Nb_2Se_9 crystal was cleaved *via* conventional peeling method.[2] It was easily separated into Nb_2Se_9 flakes adopting a quasi-two-dimensional layered structure and transferred onto a 300 nm SiO_2/Si substrate. Fig. 2 shows the SEM and AFM images of the quasi-two-dimensional Nb_2Se_9 flake with three-layer thicknesses on a 300 nm SiO_2/Si substrate.

Through weak vdW interactions, we were able to control the number of layers of the Nb_2Se_9 flakes. Fig. 3(a) shows the AFM images of several exfoliated Nb_2Se_9 flakes with different thickness on a 300 nm SiO_2/Si substrate. After the second peeling process at the same position using blue tape, the thickness of flakes reduced from 160 to 107 nm (P1 to P1′), and from 80 to 30 nm (P2 to P2′), as shown in Fig. 3(b) and (c).

An isolated monolayer of Nb_2Se_9 can be obtained on the 300 nm SiO_2/Si substrate after multiple peeling processes. Fig. 4 shows the quasi-two-dimensional structure of Nb_2Se_9 with a single chain thickness and a width of approximately 200 nm (Fig. 3(b)). Because Nb_2Se_9 is composed of single chains of Nb_2Se_9 without dangling bonds, it is likely that the exfoliated quasi-two-dimensional Nb_2Se_9 would exhibit ideal transport characteristics without degradation caused by edge scattering.
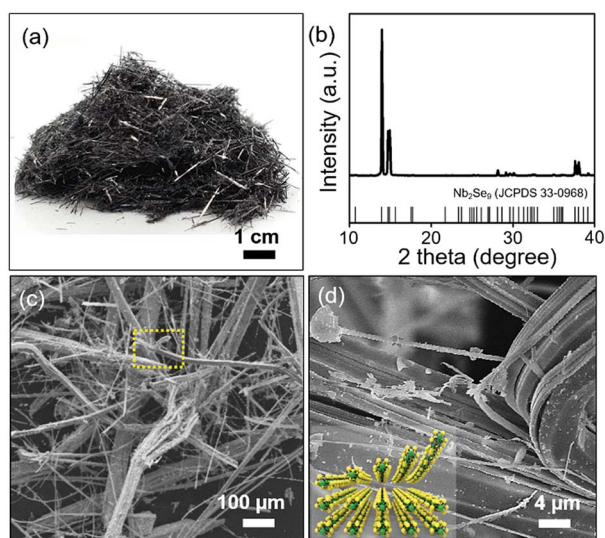

Fig. 1 (a) Photograph of the mass-production of needle-like Nb_2Se_9 crystals; (b) XRD pattern of the Nb_2Se_9 crystal; (c) and (d) low- and high-magnification SEM images of the Nb_2Se_9 crystal. The inset shows an illustration of the crystal structure of Nb_2Se_9.
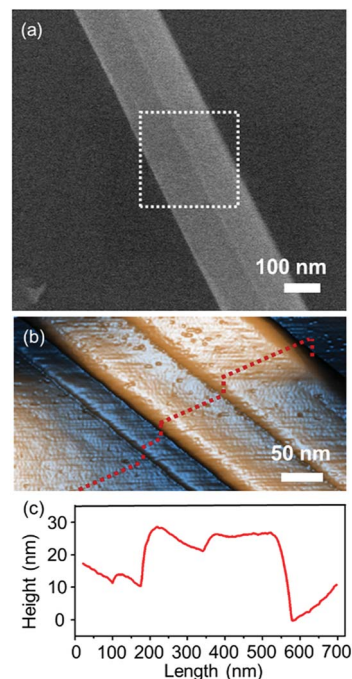
**Fig. 2** (a) SEM and (b) 3D AFM images of the exfoliated quasi-two-dimensional Nb_2Se_9 flake on a 300 nm SiO_2/Si substrate. (c) Line profile of the corresponding Nb_2Se_9 flakes, as marked in (b).
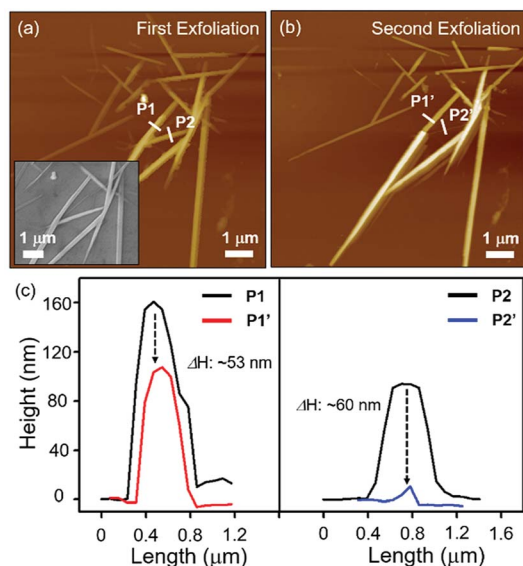
Fig. 3 (a) AFM image of the exfoliated quasi-two-dimensional Nb$_2$Se$_9$ flakes on a 300 nm SiO$_2$/Si substrate. (b) AFM image of the exfoliated Nb$_2$Se$_9$ flakes on a 300 nm SiO$_2$/Si substrate after an additional peeling process. (c) Line profile of the Nb$_2$Se$_9$ flakes before and after a second exfoliation.
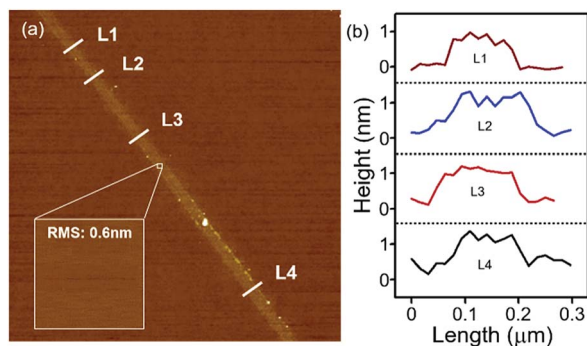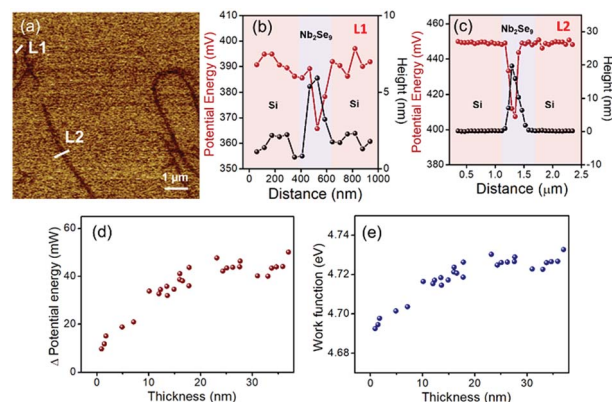

Fig. 4 AFM image of exfoliated quasi-two-dimensional monolayer Nb$_2$Se$_9$ on 300 nm SiO$_2$/Si substrate. The inset shows the HR-AFM image of selected regions and its RMS value. (b) Line profile of quasi-two-dimensional monolayer Nb$_2$Se$_9$ ribbon as marked L1, L2, L3, and L4 in (a).

The electrical properties of the Nb$_2$Se$_9$ flakes with different thicknesses were investigated by SKPM analysis. SKPM is a non-destructive analytical tool that can probe the local surface potential energy and work function by measuring the contact potential difference between the tip and sample (V$_{\mathrm{CPD}}$).[31,32] Since the Nb$_2$Se$_9$ flakes were adhered onto a Si substrate, the work can be calculated using the following equation:

$$V_{\mathrm{CPD}} = \frac{1}{e}\left(\varphi_{\mathrm{t}} - \varphi_{\mathrm{f}}\right),$$

$$\Delta V_{\mathrm{CPD}} = V_{\mathrm{CPD}}(\mathrm{Nb_2Se_9}) - V_{\mathrm{CPD}}(\mathrm{substrate})$$
$$= \frac{1}{e}\left(\varphi_{\mathrm{t}} - \varphi_{\mathrm{f}}\right) - \frac{1}{e}\left(\varphi_{\mathrm{t}} - \varphi_{\mathrm{s}}\right)$$
$$= \frac{1}{e}\left(\varphi_{\mathrm{s}} - \varphi_{\mathrm{f}}\right)$$

Fig. 5 (a) SKPM image of the exfoliated Nb$_2$Se$_9$ flakes on an Si substrate; (b) and (c) height and potential energy profiles of the Nb$_2$Se$_9$ flakes and Si substrate, as marked in (a); (d) and (e) variation of the potential energy difference and work function according to the thickness of the Nb$_2$Se$_9$ flakes.

where φ_{t}, φ_{s}, and φ_{f} represent the contact potential difference and work functions of the tip, Si substrate, and Nb$_2$Se$_9$ flakes, respectively.

As shown in Fig. 5(a), the distribution of the surface potential energy was homogeneous over the entire surface of each flake, but its value varied depending on its thickness. The surface potential energy difference between 5 nm (L1, 5–6 layers) and 20 nm (L2, approximately 20–22 layers) thick Nb$_2$Se$_9$ flakes and the Si substrate were 20 and 40 mV, respectively (Fig. 5(b) and (c)). The statistical results of >28 samples show that both the surface potential energy difference and work function begin to decrease as the thickness of the Nb$_2$Se$_9$ flakes decreases to <20 nm due to interlayer screening effects, which were also observed in typical layered materials (Fig. 5(d) and (e)).[31] The surface of the Si substrate was covered by a naturally formed hydrophilic Si oxides, generating large numbers of charge trapping sites. These sites strongly influenced the charge transfer behavior between the Nb$_2$Se$_9$ and Si substrate. Since the effective length of the interlayer screening effects increases with decreasing flake thickness, the potential energy difference and work function decreased compared to that of the bulk Nb$_2$Se$_9$.

To evaluate the electrical characteristics of the isolated Nb$_2$Se$_9$ flake, we performed electrical transport measurements of single Nb$_2$Se$_9$ field effect transistor (FET) (Fig. 6). The current–voltage (I_{ds}–V_{ds}) curve at various gate voltage (V_{g}) and current–gate voltage (I_{ds}–V_{g}) curve exhibited p-type field effect transistor characteristics (Fig. 6(b) and (c)). The transconductance (g_{m}) and field effect electron mobility (μ_{e}) were determined from the I_{ds}–V_{g} with the drain bias of 4 V in Fig. 6(b) using the following equations: $g_{\mathrm{m}} = \mathrm{d}I_{\mathrm{ds}}/\mathrm{d}V_{\mathrm{g}}$, at the maximum slope of the I_{ds}–V_{g} curve in the linear region and $\mu_{\mathrm{e}} = g_{\mathrm{m}}L^2/C_{\mathrm{ox}}V_{\mathrm{ds}}$, where L is the gate length and C is the gate capacitance of a Nb$_2$Se$_9$ flake.[33] The oxide capacitance (C_{ox}) per unit area (for the 300 nm SiO$_2$/Si substrate, $C_{\mathrm{ox}} = 0.2301$ fF). The extracted g_{m} and μ_{e} values for the Nb$_2$Se$_9$ FET are 12.9 pS and 0.0035 cm^2 V^{-1} s^{-1}.
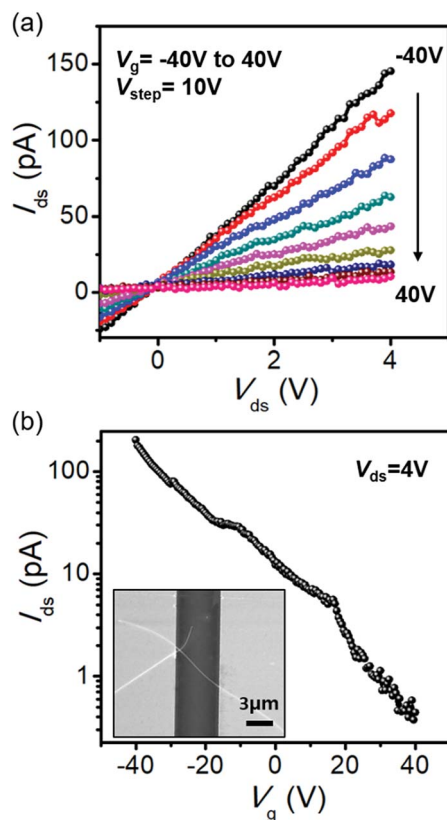
Fig. 6 (a) Current–voltage (I_{ds}–V_{ds}) characteristics of the Nb_2Se_9 FET. (b) Transfer characteristics (I_{ds}–V_g) of the Nb_2Se_9 FET. $V_g = -40$ V to 40 V. Inset shows SEM image of the Nb_2Se_9 FET.

Conclusions

In this study, layered 1D Nb_2Se_9 was successfully synthesized *via* niobium–selenium solid-state reaction on a bulk scale. Typical mechanical cleavage afforded a needle-like single crystal Nb_2Se_9 composed of numerous single Nb_2Se_9 chains linked by weak vdW interactions. The isolated Nb_2Se_9 flakes exhibited a quasi-two-dimensional layered structure whose thickness can be controlled by the repeated peeling method. The work function varied as a function of Nb_2Se_9 flake thickness as determined by SKPM measurements. In particular, the Nb_2Se_9 FET clearly exhibited p-type semiconductor characteristics with hole mobility of 0.0035 cm^2 V^{-1} s^{-1}. We believe that this novel 1D Nb_2Se_9 represents an improvement over typical 2D materials and the results of the work function variation may be helpful for selecting a proper metal electrode for future Nb_2Se_9-based electronic devices.

Experimental

Synthesis

Nb_2Se_9 was synthesized using Nb (99.99%, 325 mesh, Alfa Aesar) and Se (99%, Alfa Aesar) powders. First, 2.15 mmol of Nb and 430 mmol of Se were mixed and pelletized, then sealed in a quartz tube with a neck in the middle. The evacuated quartz tube was heated to 800 °C at 2.3 °C min^{-1} for 72 h and subsequently cooled. The unreacted Se flux was then removed by dropping the Se flux onto the other side of the tube. The residual Se was sublimed in a tube furnace at 250 °C for 24 h under an Ar atmosphere.

Mechanical exfoliation

The bulk Nb_2Se_9 was placed on wafer dicing tape (BT150EKL, Nitto) and the materials were stuck several times to yield thinner-than-bulk materials. A SiO_2/Si substrate was cleaned by ultrasonication in acetone, ethanol, and deionized water for 15 min, followed by heating at 100 °C to remove moisture from the SiO_2/Si surface. The polymer tape was strongly pressed against and adhered to and the SiO_2/Si substrate. After adhesion, the polymer tape was removed from the SiO_2/Si substrate and this process was repeated for exfoliation.

Characterization

Powder X-ray diffraction (XRD, Mac Science, M18XHF22) was performed using Cu-Kα radiation ($\lambda = 0.154$ nm). Field emission-scanning electron microscopy (FE-SEM, Hitachi, S4300SE) and atomic force microscopy (AFM, Park systems, NX 10) were performed in a non-contact mode for the topographic analysis of the mechanically exfoliated Nb_2Se_9 on the substrate. SKPM (Park systems, NX10) measurements were performed using Si tips coated by Cr–Pt (Multi75-G, Budget Sensors Inc.) with a resonance frequency of 75 kHz, a scan rate of 0.3 Hz, and a sample bias of ± 1 V.

Device fabrication

The Nb_2Se_9 FET was fabricated by conventional photolithography using p^+ Si (100) wafer with a 300 nm thick SiO_2 layer on top.[33] Metal electrodes were pattered and deposited using thermal evaporator in an ultra-high vacuum (20 nm Cr and 200 nm Au, ~10^{-6} Torr). The conducting channel length, width, and the thickness of the Nb_2Se_9 flake is 5 μm, 400 nm, and 70 nm, respectively (Fig. S2†).

Conflicts of interest

There are no conflicts to declare.

Acknowledgements

Notes and references

1 X. Huang, W. C. Lee, C. Kuo, D. Hisamoto, L. Chang, J. Kedzierski, E. Anderson, H. Takeuchi, Y. K. Choi, K. Asano, V. Subramanian, T. J. King, J. Bokor and C. Hu, *IEEE Trans. Electron Devices*, 2001, **48**, 880–886.

2 K. S. Novoselov, A. K. Geim, S. V. Morozov, D. Jiang, M. I. Katsnelson, I. V. Grigorieva, S. V. Dubonos and A. Firsov, *Nature*, 2005, **438**, 197–200.

3 B. Radisavljevic, A. Radenovic, J. Brivio, I. V. Giacometti and A. Kis, *Nat. Nanotechnol.*, 2011, **6**, 147–150.

4 A. K. Geim and I. V. Grigorieva, *Nature*, 2013, **499**, 419–425.

5 Y. Zhang, Y.-W. Tan, H. L. Stormer and P. Kim, *Nature*, 2005, **438**, 201–204.

6 C. Lee, X. Wei, J. W. Kysar and J. Hone, *Science*, 2008, **321**, 385–388.

7 Y. W. Son, M. L. Cohen and S. G. Louie, *Nature*, 2006, **444**, 347–349.

8 P. Avouris, Z. Chen and V. Perebeinos, *Nat. Nanotechnol.*, 2007, **2**, 605–615.

9 Y. Zhang, T. T. Tang, C. Girit, Z. Hao, M. C. Martin, A. Zettl, M. F. Crommie, Y. R. Shen and F. Wang, *Nature*, 2009, **459**, 820–823.

10 J. Qiao, X. Kong, Z. X. Hu, F. Yang and W. Ji, *Nat. Commun.*, 2014, **5**, 4474.

11 A. Castellanos-Gomez, L. Vicarelli, E. Prada, J. O. Island, K. L. Narasimha-Acharya, S. I. Blanter, D. J. Groenendijk, M. Buscema, G. A. Steele, J. V. Alvarez, H. W. Zandbergen, J. J. Palacios and H. S. J. Van Der Zant, *2D Materials*, 2014, **1**, 025001.

12 A. S. Mayorov, R. V. Gorbachev, S. V. Morozov, L. Britnell, R. Jalil, L. A. Ponomarenko, P. Blake, K. S. Novoselov, K. Watanabe, T. Taniguchi and A. K. Geim, *Nano Lett.*, 2011, **11**, 2396–2399.

13 F. Schwierz, *Nat. Nanotechnol.*, 2010, **5**, 487–496.

14 P. Avouris, M. Freitag and V. Perebeinos, *Nat. Photonics*, 2008, **2**, 341–350.

15 J. Wang and M. Musameh, *Anal. Chem.*, 2003, **75**, 2075–2079.

16 M. Kusunoki, T. Suzuki, C. Honjo, T. Hirayama and N. Shibata, *Chem. Phys. Lett.*, 2002, **366**, 458–462.

17 D. N. McCarthy, V. Nicolosi, D. Vengust, D. Mihailovic, G. Compagnini, W. J. Blau and J. N. Coleman, *J. Appl. Phys.*, 2007, **101**, 014317.

18 J. H. Golden, F. J. DiSalvo, J. M. J. Fréchet, J. Silcox, M. Thomas and J. Elman, *Science*, 1996, **273**, 782–784.

19 B. Messer, J. H. Song, M. Huang, Y. Wu, F. Kim and P. Yang, *Adv. Mater.*, 2000, **12**, 1526–1528.

20 A. Heidelberg, H. Bloeß, J. W. Schultze, C. J. Booth, E. T. Samulski and J. J. Boland, *Z. Phys. Chem.*, 2003, **217**, 573–585.

21 F. E. Osterloh, H. Hiramatsu, R. K. Dumas and K. Liu, *Langmuir*, 2005, **21**, 9709–9713.

22 A. Meden, A. Kodre, J. P. Gomilšek, I. Arčon, I. Vilfan, D. Vrbanic, A. Mrzel and D. Mihailovic, *Nanotechnology*, 2005, **16**, 1578–1583.

23 N. Sun, M. McMullan, P. Papakonstantinou, H. Gao, X. Zhang, D. Mihailovic and M. Li, *Anal. Chem.*, 2008, **80**, 3593–3597.

24 M. I. Ploscaru, S. J. Kokalj, M. Uplaznik, D. Vengust, D. Turk, A. Mrzel and D. Mihailovic, *Nano Lett.*, 2007, **7**, 1445–1448.

25 Y. Zhou, L. Wang, S. Chen, S. Qin, X. Liu, J. Chen, D. J. Xue, M. Luo, Y. Cao, Y. Cheng, E. H. Sargent and J. Tang, *Nat. Photonics*, 2015, **9**, 409–415.

26 X. Xu, S. Jeong, C. S. Rout, P. Oh, M. Ko, H. Kim, M. G. Kim, R. Cao, H. S. Shin and J. Cho, *J. Mater. Chem. A*, 2014, **2**, 10847–10853.

27 S. Britto, M. Leskes, X. Hua, C. A. Hébert, H. S. Shin, S. Clarke, O. Borkiewicz, K. W. Chapman, R. Seshadri, J. Cho and C. P. Grey, *J. Am. Chem. Soc.*, 2015, **137**, 8499–8508.

28 A. Meerschault, L. Guema, R. Berger and J. Rouxel, *Acta Crystallogr., Sect. B: Struct. Crystallogr. Cryst. Chem.*, 1979, **35**, 1747–1750.

29 S. A. Sunshine and J. A. Ibers, *Acta Crystallogr., Sect. C: Cryst. Struct. Commun.*, 1987, **43**, 1019–1022.

30 R. Sanjines, H. Berger and F. Levy, *Mater. Res. Bull.*, 1988, **23**, 549–553.

31 N. J. Lee, J. W. Yoo, Y. J. Choi, C. J. Kang, D. Y. Jeon, D. C. Kim, S. Seo and H. J. Chung, *Appl. Phys. Lett.*, 2009, **95**, 222107.

32 S. H. Choi, Z. Shaolin and W. Yang, *J. Korean Phys. Soc.*, 2014, **64**, 1550–1555.

33 J. H. Lee, B.-S. Kim, S.-H. Choi, Y. Jang, S. W. Hwang and D. Whang, *Nanoscale*, 2013, **5**, 8968–8972.